

Estimation of the crustal structure in Central Anatolia (Turkey) using receiver functions

Begüm ÇIVGIN*, Bülent KAYPAK

Department of Geophysical Engineering, Faculty of Engineering, Ankara University, Ankara, Turkey

Received: 16.03.2017 • Accepted/Published Online: 09.08.2017 • Final Version: 29.09.2017

Abstract: The receiver function analysis method was used to determine the crustal structure in Central Anatolia, Turkey, by using teleseismic earthquake records. The method is based on the conversion of incident P waves into S waves reaching an interface in the crust or upper mantle and arrival of the converted wave to the station just after the direct P waves. A temporary seismic network, the Ankara Earthquake Monitoring Network (AnkNET), consisting of six broadband seismograph stations, has been deployed in order to monitor the seismicity in Ankara and its surroundings during the period of 2007–2010. In this study, the crustal structures beneath AnkNET stations were investigated. The stations were located between latitudes 39°N and 41°N and longitudes 32°E and 34°E about 100 km apart from each other around a circle with a radius of about 100 km, including one in Ankara approximately in the center. Hypocentral parameters of 43 teleseismic earthquakes equal to or greater than an instrumental magnitude M_w of 6.5 that occurred at a distance between 30° and 100° far from the central coordinates of AnkNET (40°N, 33°E) were retrieved from the Incorporated Research Institutions for Seismology earthquake catalogue. According to the results of this study, the crustal thickness of the region is between 34.5 km and 40.5 km and the S-wave velocity varies between 3.3 km/s and 4.1 km/s. It is expected that the calculated crustal thickness and velocity values will contribute to future studies in the region.

Key words: Crustal structure, crustal thickness, H-K stack, receiver functions, S-wave velocity structure, teleseismic earthquakes, V_p/V_s ratio

1. Introduction

The region called Central Anatolia is a part of the Anatolian plate, bordered between the North Anatolian Fault zone (NAFZ) and the East Anatolian Fault zone (EAFZ) (Figure 1a). The Anatolian plate moves westwards, turning counterclockwise along the Bitlis-Zagros suture zone (BSZS) due to the north-northwest movement of the Arabian plate and the northward movement of the African plate relative to the Eurasian plate (e.g., McKenzie, 1972; Ergün et al., 1995; McClusky et al., 2000).

The crustal structure of Central Anatolia has been studied by various researchers and several models have been developed. Some of them assert that the crustal thickness of the Anatolian plate gets thinner from east to west (e.g., Marone et al., 2003; Angus et al., 2005; Luccio and Pasyanos, 2007; Maden et al., 2008). Marone et al. (2003) determined that the mean crustal thickness in Central Anatolia varies between 36 and 40 km. Arslan et al. (2010) studied the crustal structure of Turkey using gravity data and found results very similar to those of Marone et al. (2003). They declared that the crust gets thinner towards the northwest as a result of their study. Vanacore et al. (2013) indicate that the Moho depth

beneath Central Anatolia is approximately 37 km in their study based on receiver function analysis. In a similar study by Tezel et al. (2013), the crustal thickness in Central Anatolia varies between 31 km and 38 km. Uluocak et al. (2016) determined the crustal thickness in our study region to be between 35 km and 36 km. The crustal thickness beneath the study area varies between 35 km and 36.5 km in Crust1.0, the crustal model of Laske et al. (2013). The crustal model of Molinari and Morelli (2011), EPCrust, gives a wider range between 36 km and 42.5 km. Luccio and Pasyanos (2007) indicated that the crustal S-wave velocity of Turkey varies between 3.4 km/s and 3.7 km/s, rising to 3.9 km/s in Central Anatolia and reaching 4 km/s near the East Anatolian Fault. They concluded that the crustal thickness reaches 50 km beneath Central Anatolia. There are several studies presenting the crustal structure beneath a commonly used permanent station, ANTO (39.87°N, 32.79°E), located within the study area. Türkelli (1984) used ANTO seismograms to determine the crustal and upper mantle structure beneath the city of Ankara. He utilized the Thomson–Haskell matrix method to determine the crustal structure and obtained 30 km of thickness for the crust. Türkelli (1984) concluded that

* Correspondence: begum.koca@eng.ankara.edu.tr

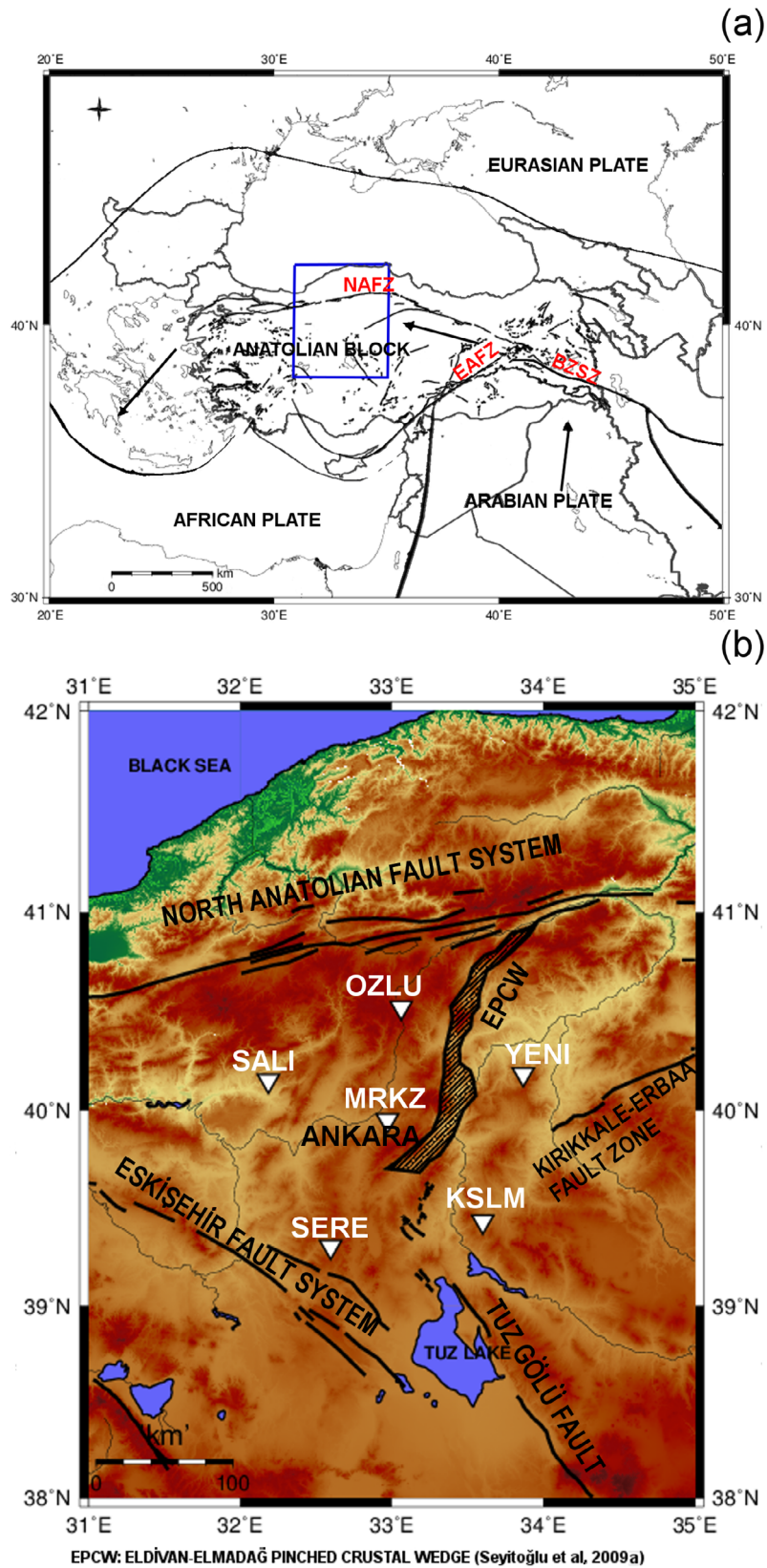


Figure 1. (a) Main tectonic features around the study area and (b) location map of the six 3-component broadband stations of the temporary network AnkNET (white triangles).

the crustal thickness beneath the ANTO station is 30 km. Sandvol et al. (1998) studied the Moho depth beneath the ANTO station by using receiver function analysis. They concluded that the crustal thickness under the ANTO station is 37 km. In a similar study carried out by Saunders et al. (1998), a gradational Moho between 34 and 38 km in depth is proposed. Zhu et al. (2006) estimated the Moho depth beneath ANTO as 36 km and found that the crustal thickness tapers off towards the Aegean Sea to 25 km. Gürbüz et al. (2003) declared that the crustal thickness is 36 km beneath Keskin, Kırıkkale (located within the research area).

Waveforms of the body waves generated by distant earthquakes are being used in the receiver function method to provide information about the discontinuities in the crust and upper mantle beneath seismic stations with three components (e.g., Langston, 1977; Owens et al., 1984; Kind and Vinnik, 1988; Ammon, 1991). These waveforms contain the knowledge of source time function, effect of propagation through the mantle, and the local structure beneath the station. Teleseismic earthquake records are being used in this method, which is based on the conversion of incident P waves into S waves reaching an interface in the crust or in the upper mantle and arrival of the converted wave to the station just after the direct P waves.

In this study, the receiver function analysis method was utilized to determine the crustal structure in the vicinity of Ankara, Central Anatolia. The waveform dataset was obtained from a local temporary seismic network called AnkNET (Ankara Seismic Network; Seyitoğlu et al., 2009a), operated between 10 September 2007 and 23 September 2010. The main objective of this network was to carry out seismological studies and put forth the subsurface structure of this region. One important issue of such a study is to determine the crustal seismic velocity structure. The motivation of this study was to determine the crustal structure of the region by using the receiver function analysis method. Some of the above-referred studies utilized receiver function traces of teleseismic events to estimate the structure of the crust and mantle beneath significant stations in Central Anatolia. The main objective of this study is to investigate the crustal structure of the areas in which no seismic stations have been employed formerly.

2. Data

The teleseismic earthquake data recorded by the temporary local seismograph network, AnkNET, were used to estimate the crustal thickness. Location of the AnkNET stations and the main tectonic features in the vicinity of the study area are shown in Figure 1b. AnkNET consisted of six three-component broadband seismometers located

in the Central Anatolia region, around the city of Ankara. One of the stations was located in the city of Ankara (MRKZ station) and the other five were located around Ankara at about 100 km from each other. The radius of the network was about 100 km.

Teleseismic earthquakes that occurred at an epicentral distance between 30° and 100° from the center of the network were selected. Data recorded at each station have been investigated in terms of their noise levels, and the records with low signal-to-noise ratio were removed. Numbers of data used at each station are as follows: KSLM - 28, MRKZ - 26, OZLU - 23, SALI - 34, SERE - 29, and YENI - 26. Distribution of the teleseismic events used for the receiver function analysis and their distances from the AnkNET network are shown in Figure 2. Hypocentral parameters of the 43 earthquakes (Table 1) of Mw 6.5 or greater that occurred at epicentral distances between 30° and 100° from the center of AnkNET (40°N , 33°E) were retrieved from the Incorporated Research Institutions for Seismology (IRIS) earthquake catalogue (retrieved 15 September 2009 from http://ds.iris.edu/wilber3/find_event).

3. Receiver functions

The receiver function analysis method is based on the conversion of the P wave into the S wave when it arrives at an interface in the crust or upper mantle. This converted phase arrives to the station just after the direct P wave. A simple receiver function trace of a two-layered model and

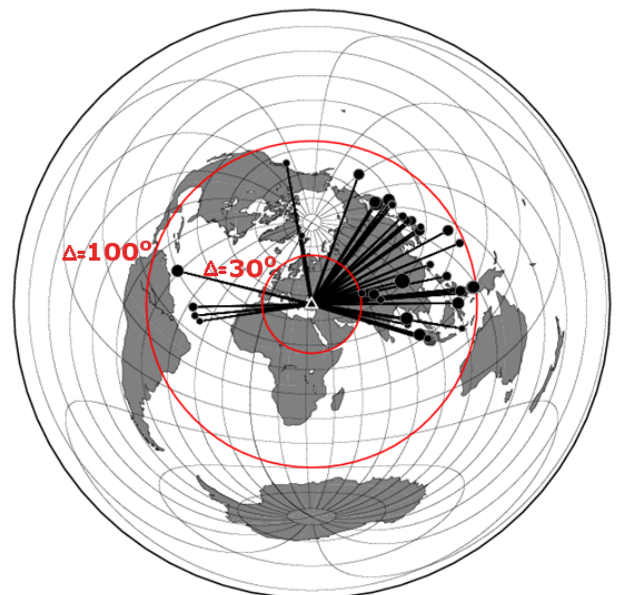


Figure 2. Location map of the teleseismic events (bullets) used in the receiver function analysis and their distances to the center of the Ankara Seismic Network (triangle). Straight lines represent the symbolic ray paths from teleseismic events to the network.

Table 1. Hypocentral parameters of the earthquakes used in receiver function analysis. Δ is the epicentral distance of the earthquake to the center of the AnkNET (40°N, 33°E) station network.

No.	Date	Origin time	Latitude (°)	Longitude (°)	Depth (km)	M_w	Δ (°)	Back azimuth
1	24.10.2007	21:02:50.6	-3.90	101.02	21	6.8	76.028	107.4
2	31.10.2007	03:30:16.0	18.90	145.39	207	7.2	93.955	61.4
3	25.11.2007	16:02:15.8	-8.29	118.37	20	6.5	91.867	99.3
4	25.11.2007	19:53:05.5	-8.22	118.47	18	6.5	91.898	99.2
5	29.11.2007	19:00:20.4	14.94	-61.27	156	7.4	83.707	284.2
6	19.12.2007	09:30:27.9	51.36	-179.51	34	7.2	84.394	19.9
7	05.01.2008	11:01:06.1	51.25	-130.75	15	6.6	87.712	349.9
8	08.02.2008	09:38:14.1	10.67	-41.90	9	6.9	71.681	236.3
9	20.02.2008	08:08:30.5	2.77	95.96	26	7.4	67.780	106.0
10	24.02.2008	14:46:21.5	-2.40	99.93	22	6.5	74.208	107.2
11	25.02.2008	08:36:33.0	-2.49	99.97	25	7.2	74.299	107.2
12	25.02.2008	18:06:03.9	-2.33	99.89	25	6.6	74.131	107.2
13	25.02.2008	21:02:18.4	-2.24	99.81	25	6.7	74.011	107.1
14	03.03.2008	09:31:02.5	46.41	153.18	10	6.5	78.514	37.5
15	03.03.2008	14:11:14.6	13.35	125.63	24	6.9	83.498	79.0
16	20.03.2008	22:32:57.9	35.49	81.47	10	7.2	38.146	80.6
17	09.05.2008	21:51:29.7	12.52	143.18	76	6.8	96.879	67.5
18	12.05.2008	06:28:01.6	31.00	103.32	19	7.9	56.521	75.4
19	23.05.2008	19:35:34.8	7.31	-34.90	8	6.5	68.476	261.3
20	13.06.2008	23:43:45.4	39.03	140.88	7	6.9	77.222	49.4
21	27.06.2008	11:40:14.0	11.01	91.82	17	6.6	59.239	102.0
22	05.07.2008	02:12:04.5	53.88	152.89	632	7.7	72.940	32.4
23	19.07.2008	02:39:28.7	37.55	142.21	22	7.0	78.989	49.8
24	23.07.2008	15:26:20.0	39.80	141.46	108	6.8	77.044	48.5
25	25.08.2008	13:21:58.8	30.90	83.52	12	6.7	41.609	86.1
26	10.09.2008	13:08:14.7	8.09	-38.71	9	6.6	70.872	264.5
27	11.09.2008	00:00:02.7	1.88	127.36	96	6.6	92.190	85.8
28	11.09.2008	00:20:50.9	41.89	143.75	25	6.8	76.923	45.7
29	05.10.2008	15:52:49.4	39.53	73.82	27	6.7	31.123	77.2
30	16.11.2008	17:02:32.7	1.27	122.09	30	7.4	88.547	89.5
31	24.11.2008	09:02:58.8	54.20	154.32	492	7.3	73.287	31.3
32	03.01.2009	19:43:50.7	-0.41	132.88	17	7.6	97.885	83.7
33	03.01.2009	22:33:40.3	-0.69	133.30	23	7.4	98.387	83.6
34	15.01.2009	17:49:39.1	46.86	155.15	36	7.4	79.084	36.0
35	11.02.2009	17:34:50.8	3.88	126.40	22	7.2	90.167	84.5
36	06.03.2009	10:50:29.4	80.32	-1.85	9	6.5	42.354	351.9
37	07.04.2009	04:23:33.1	46.05	151.55	31	6.9	78.008	38.5
38	18.04.2009	19:17:58.9	46.01	151.43	35	6.6	77.980	38.4
39	09.08.2009	10:55:55.6	33.17	137.94	297	7.1	79.313	55.6
40	10.08.2009	19:55:35.6	14.10	92.89	4	7.5	58.081	98.5
41	12.08.2009	22:48:51.4	32.82	140.40	53	6.6	81.088	54.4
42	16.08.2009	07:38:21.7	-1.48	99.49	20	6.7	73.259	104.5
43	17.08.2009	00:05:49.0	23.50	123.50	20	6.7	75.563	71.4

the ray paths of the converted phase Ps and its multiples (PpPms, PpSms+PsPms) are shown in Figure 3. After the direct P-wave, the converted phase and then the multiples of it appear on the receiver function trace.

Measuring the time delay between the direct P wave and the converted Ps phase enables the determination of the seismic discontinuities beneath the stations. The converted phase and its multiples contain valuable information about the crust, such as the crustal thickness and the Vp/Vs ratio.

In order to produce the receiver functions, observed data at each station are processed individually. The first step is to remove the receiver effects by instrument correction. The instrument correction at each station is simply done by dividing the amplitudes by the amplification constant of each component. After the instrumental correction, the P waveform should be decontaminated from the presignal noise and the other seismic phases. Then the waveforms should be rotated from the original Z, north-south, and east-west (ZNE) coordinate system to the Z, radial, and transverse (ZRT) back azimuth coordinate system. Direct P-wave energy is dominant on the Z component and Ps energy dominates the R component. In this study, we used seismic analysis code (SAC; Goldstein et al., 2003; Goldstein and Snoke, 2005) to perform the instrument correction and rotation procedures. The incident angle, azimuth, back azimuth, and distance of the earthquake can be calculated automatically by SAC; it just requires the arrival time of the P wave and the incident angles and azimuths of all components added in the header of the records. The next step is to remove the effects of the source and the ray path by deconvolution of the observed vertical component from the radial component in the frequency domain (e.g., Phinney, 1964; Vinnik, 1977; Langston, 1979). The radial component of the receiver function $R(\omega)$ can be calculated by using the Fourier transforms of the radial and vertical components ($S_r(\omega)$ and $S_v(\omega)$) of the seismogram with the following equation (e.g., Langston, 1979), in which ω represents the angular frequency:

$$R(\omega) = S_r(\omega) / S_v(\omega). \tag{1}$$

This is the frequency domain equivalent of the deconvolution of vertical component displacement response from the radial component. Langston (1979) included a low-pass Gaussian filter, $G(\omega)$, in Eq. (1) in order to exclude high-frequency signals. Thus, the deconvolved radial response, $R'(\omega)$, takes the following form

$$R'(\omega) = (S_r(\omega) \times \overline{S_v(\omega)}) / (S_v(\omega) \times \overline{S_v(\omega)}) \times G(\omega), \tag{2}$$

in which $\overline{S_v(\omega)}$ is the complex conjugate of the vertical response and

$$G(\omega) = \exp(-\omega^2 / 4a^2). \tag{3}$$

The Gaussian filter-width parameter a in Eq. (3) controls the width of the low-pass Gaussian filter and can be chosen by a trial approach. The criterion determined by Langston (1979) is to produce synthetic traces that display a smooth impulse-like shape and fit the observed data in the time domain. The best-fitting Gaussian filter parameter values are 0.5, 1.0, and 2.5 in our case. The low-pass filtered radial component receiver functions with these Gaussian filter-width parameters at the KSLM station are shown in Figure 4.

It becomes difficult to pick the converted phases when the filter parameter is 0.5 and the noise level increases when it is 2.5. Similar computation of the entire receiver functions at all six stations of AnkNET was performed in order to select the optimal value of the Gaussian filter-width parameter.

4. Estimation of the S-wave velocity structure

Once the parameters for the production of the synthetic receiver functions are determined, the S-wave velocity structure beneath a station can be estimated with an iterative inversion scheme. This inversion procedure involves the

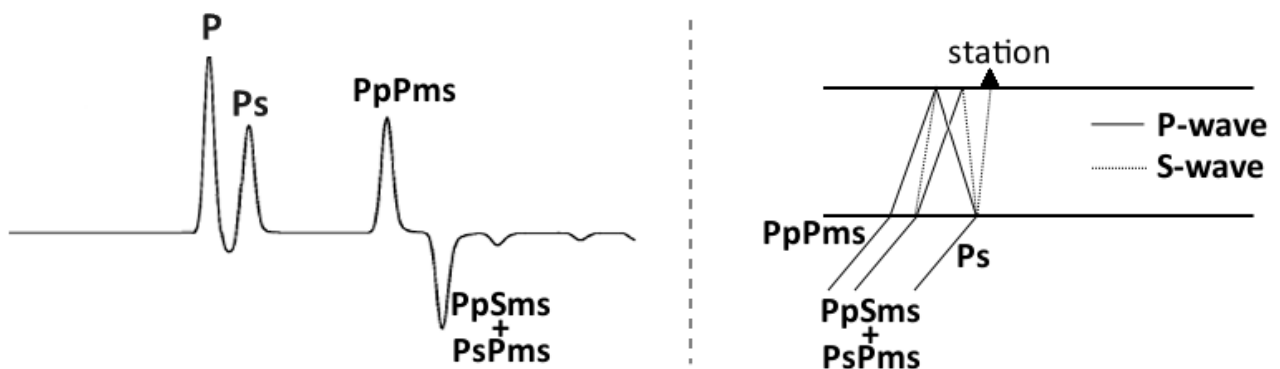


Figure 3. A simple receiver function trace for a two layered model (left) and the ray paths of the converted phase and its multiples (right). The converted phase arrives just after the direct P-wave.

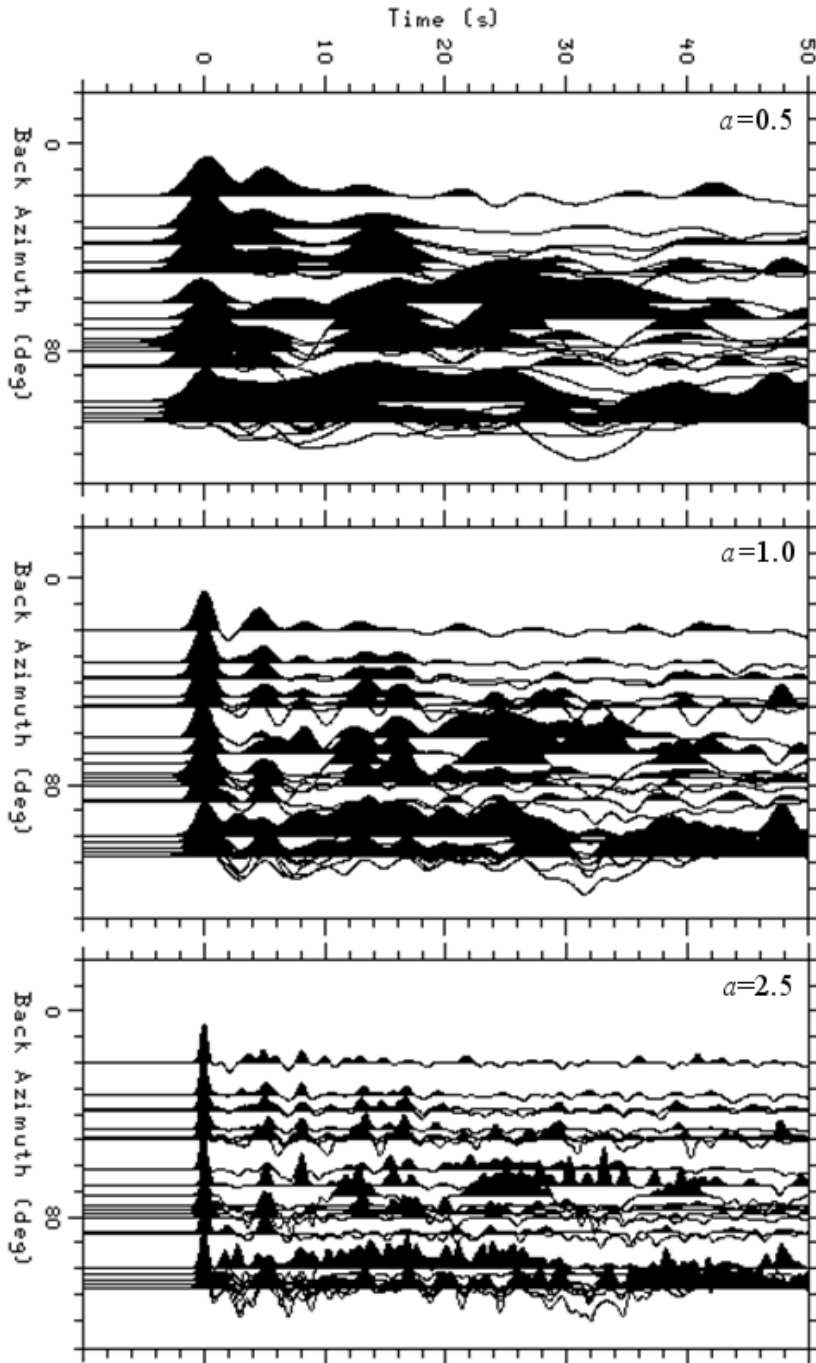


Figure 4. Some of the receiver functions calculated with three Gaussian filter-width parameter values, $a = 0.5$, $a = 1.0$, and $a = 2.5$, at the KSLM station, sorted by back azimuth.

minimization of the differences between the observed and the synthetic receiver functions. Using the a priori known seismic velocity structure as the initial model would provide reliable inversion results. A detailed description of the inversion method is given by Kind et al. (1995).

We are seeking the best-fitting synthetic receiver functions to the observed ones, with which we can

estimate the S-wave velocity model beneath the station. For this purpose, receiver functions from all events at each station were inverted using two selected Gaussian filter parameters, 1.0 and 2.5, over a 25-s time window initializing 5 s prior to the arrival of the direct P wave. The observed and synthetic receiver functions were compared by inspecting their misfit values (Figure 5).

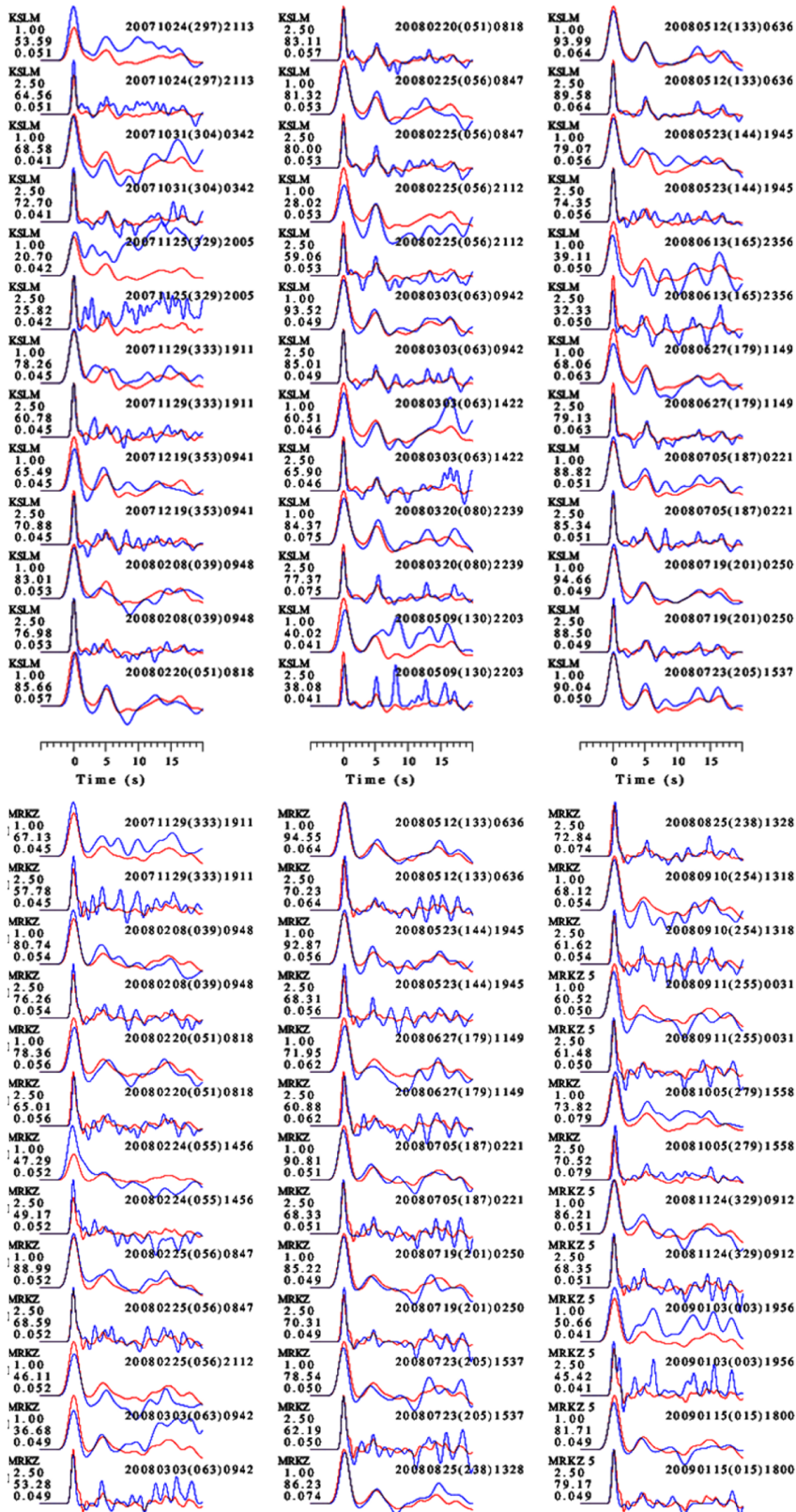


Figure 5. Synthetic (red) and observed (blue) receiver functions at all stations. Misfit between observed and synthetic receiver function is given below the station code; Gaussian filter width parameter and ray parameter are given on the left-hand side of each trace.

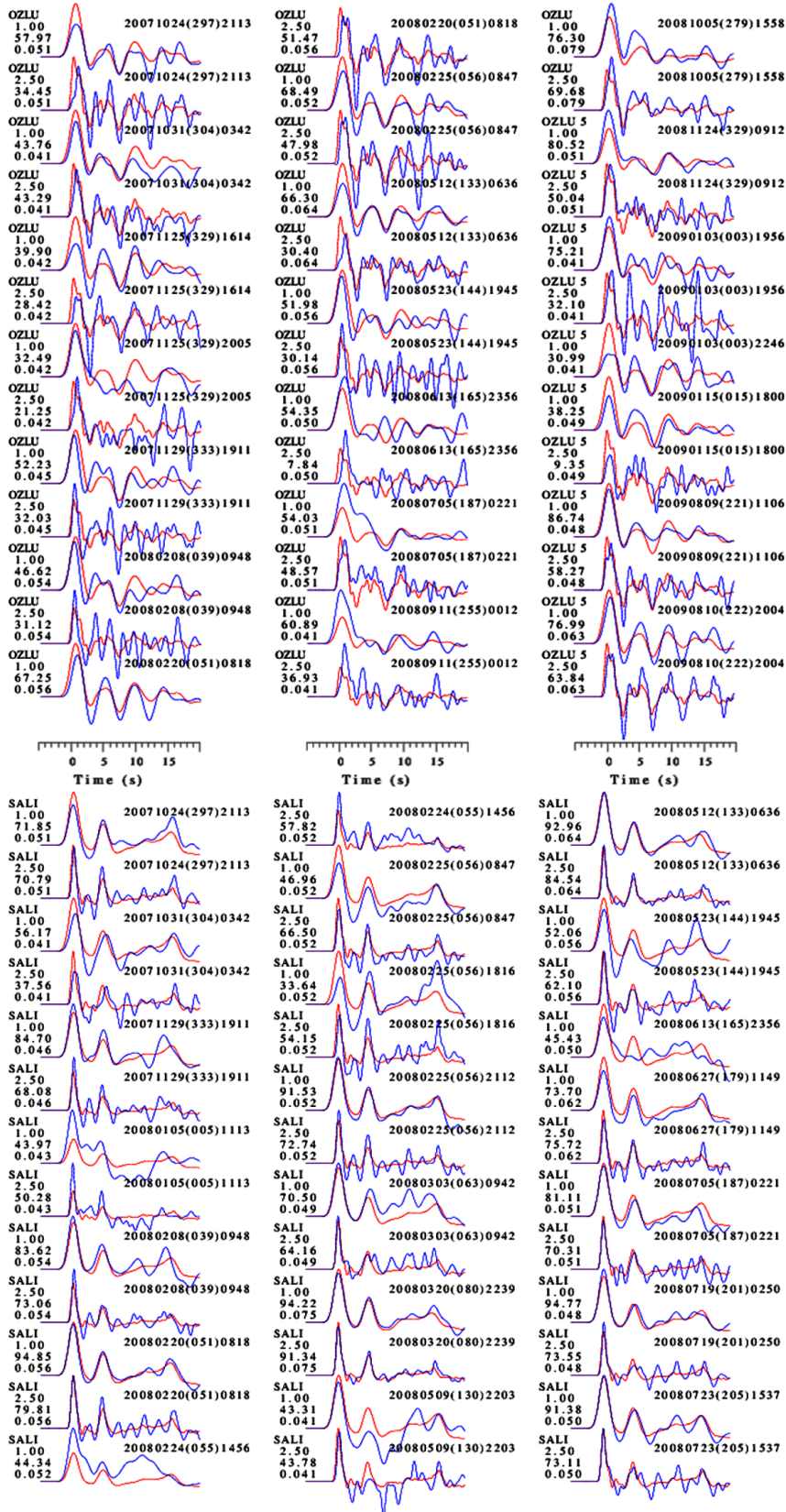


Figure 5. (Continued).

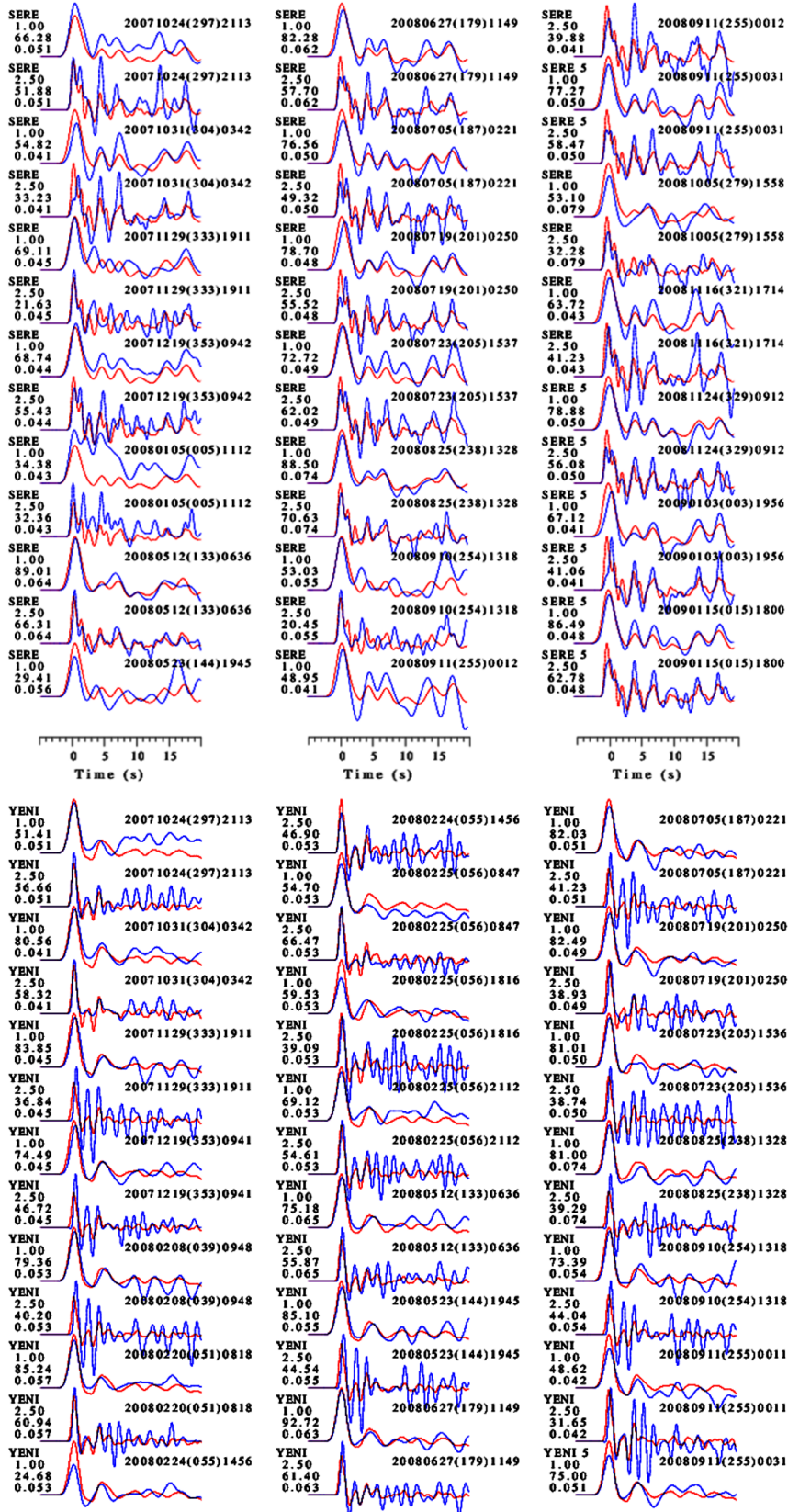


Figure 5. (Continued).

Every station has to be handled individually in the inversion process. An initial one-dimensional, isotropic S-wave velocity model is iteratively inverted to determine the one-dimensional S-wave velocity model beneath a certain station. In order to establish an initial constant-velocity layered model, a starting S-wave velocity should be selected that represents all depth levels. Following the S-wave velocity structure estimated by Tezel et al. (2007) down to 90 km depth, the starting S-wave velocity is selected as 4.5 km/s, which can represent all depths of the initial model. The upper 50 km of depth was divided into 2-km-thick layers by taking the higher anisotropy in shallow depths into consideration. The lower 50 km of depth was divided into 5-km-thick layers. The weighting factors of the inversion were selected to permit the upper 50 km to change somewhat, though the depth ranges from 50 km to 100 km were weighted moderately.

5. Estimation of the Moho depth and Vp/Vs ratio

In order to estimate the crustal thickness and the Vp/Vs ratio from the crustal P-wave velocity, arrival times of the Ps phase and the crustal multiples can be used. An algorithm called the H-K stacking method (H for crustal thickness and K for Vp/Vs ratio) was proposed by Zhu and Kanamori (2000) in order to compute the Moho depth and Vp/Vs ratio. The amplitudes of the receiver functions are stacked at the estimated arrival times of the converted phase and its multiples for various crustal thicknesses (H) and Vp/Vs ratios (K).

Delay time correction is required to accomplish the alignment and stacking of the receiver functions. The delay time correction varies with the depth of the reflector and the ray parameter of the direct P wave. The delay times of reflections from the interfaces at shallow depths are smaller than those from deep discontinuities. After delay time corrections, the converted phases make a straight line and the multiples make an inclined line when the signals are aligned. Alignment of the receiver functions enables us to distinguish the converted phases from the multiples.

The time pick of the Moho converted phase and its multiples is not required in the H-K method. The following weighting and stacking procedure is performed for every station individually.

$$S(H,K) = w_1 Q(t_1) + w_2 Q(t_2) + w_3 Q(t_3) \quad (4)$$

Receiver functions are weighted with the factors w_1 , w_2 , and w_3 for the phases Ps, PpPms, and PpSms+PsPms respectively by multiplying the amplitudes of the receiver functions ($Q(t_i)$) of the corresponding phases. The arrival times (t_1 , t_2 , and t_3) of Ps, PpPms, and PpSms+PsPms are estimated for the given values of H and K. The most important advantage of this method is to assume that the

value of $S(H,K)$ reaches its maximum with the true H and K values.

Arrival time of the converted phase Ps is given by:

$$t_{ps} = H \times ((Vs^2 - p^2)^{1/2} - (Vp^2 - p^2)^{1/2}), \quad (5)$$

where H is the depth of the discontinuity, Vp and Vs are P- and S-wave velocities, and p is the ray parameter, which is assumed to be equal for both the direct P wave and the Ps converted phase. Similarly, arrival times of the multiples PpPms and PpSms+PsPms can be calculated with the following equations, respectively:

$$t_{ppps} = H \times ((Vs^2 - p^2)^{1/2} + (Vp^2 - p^2)^{1/2}), \quad (6)$$

$$t_{ppss+ppps} = 2 \times H \times (Vs^2 - p^2)^{1/2}. \quad (7)$$

The $S(H,K)$ values are calculated over an H-K space with the specified Moho depth and Vp/Vs ratio intervals. The amplitudes of $S(H,K)$ at each node of the H-K space are stacked using Eq. (4).

The uncertainties of H and K were calculated using the equations given by Zhu and Kanamori (2000):

$$\sigma_H^2 = 2 \times \sigma_s^2 / \partial^2 S / \partial H^2, \quad (8)$$

$$\sigma_K^2 = 2 \times \sigma_s^2 / \partial^2 S / \partial K^2, \quad (9)$$

where σ_s^2 is the variance of $S(H,K)$.

6. Inversion results

The starting models to be inverted for the S-wave velocity were calculated by using a constant (4.5 km/s) S-wave isotropic one-dimensional model. The time window for inversion was set to 5 s before and 20 s after the first arrival of the direct P wave for the receiver functions with Gaussian filter width parameters of 1.0 and 2.5. At the end of 30 iterations, the observed and synthetic receiver functions were compared by inspecting their misfit values (Figure 5). The velocity model is refined iteratively to reduce the misfit between synthetic and observed receiver functions. The initial, trial, and final 1-D S-wave velocity models beneath the six stations of AnKNET are shown in Figure 6. Trial models appear to tend to approach the final model and show the main seismic discontinuities beneath the stations from the first iteration. S-wave velocity models beneath the stations show that the crust–mantle boundaries agree well with those determined by using the H-K stacking method. The $S(H,K)$ values were calculated over an H-K space with 0.1 km Moho depth intervals changing between 20 and 45 km and Vp/Vs ratios changing between 1.5 and 2.0 with intervals of 0.002. Weighting factors $w_1 = 0.6$, $w_2 = 0.3$, and $w_3 = 0.1$ for phases Ps, PpPms, and PpSms+PsPms,

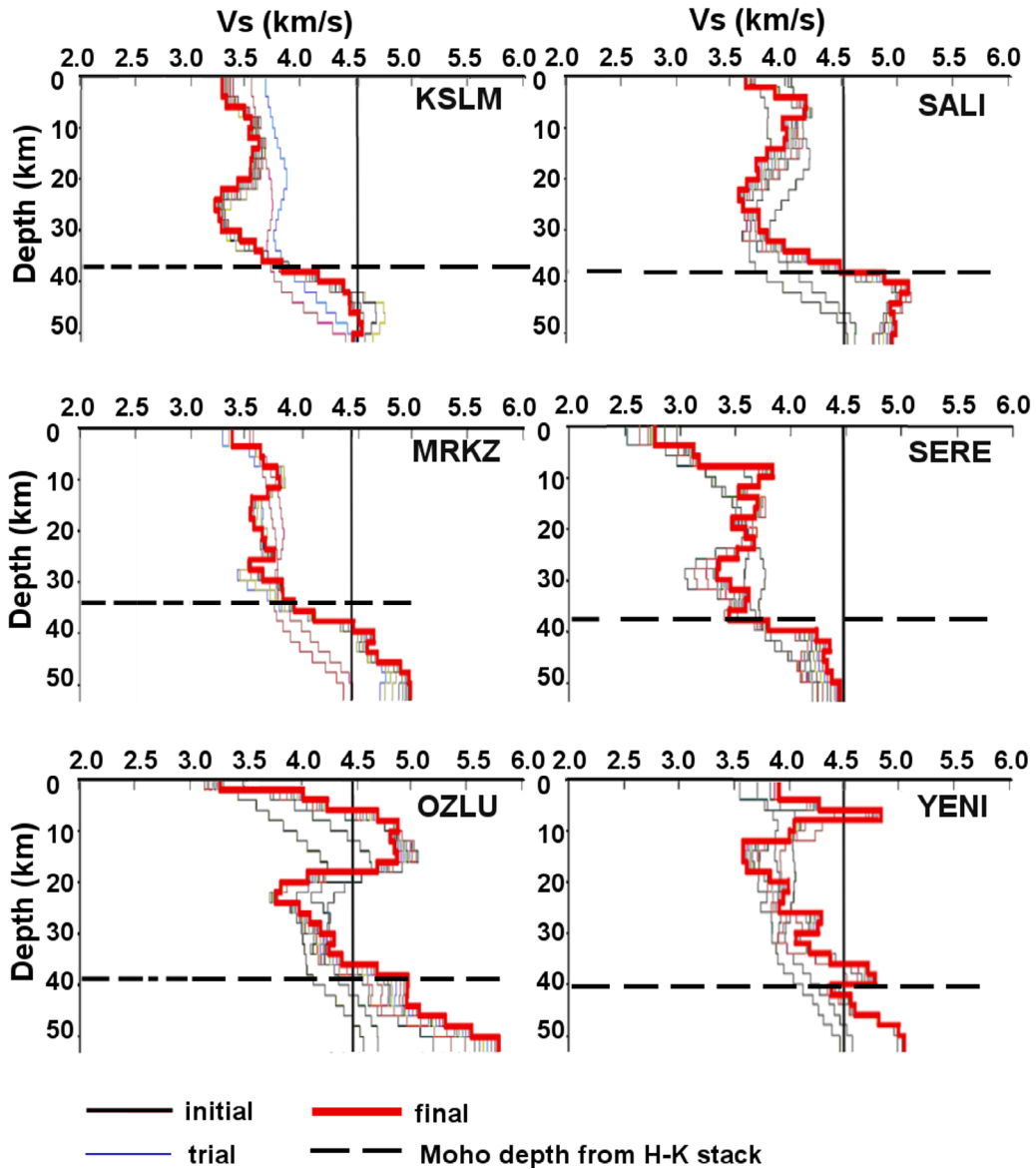


Figure 6. Initial, trial, and final 1-D S-wave velocity models beneath the six stations of AnkNET. Moho depths from H-K stacking are also shown.

respectively, were chosen to meet $\sum w_i = 1$, $i = 1, 2, 3$ and to equilibrate the contributions of all phases. Locations of the stations, crustal thicknesses without station elevation correction and V_p/V_s ratios from H-K stacking, Poisson's ratio (σ), and mean crustal S-wave velocities are given in Table 2.

The H-K stack for stations MRKZ, OZLU, and SALI clearly indicates the real values of H and V_p/V_s with one maximum $S(H,K)$ value (Figure 7). At the MRKZ station the crustal thickness H is 34.5 km and the V_p/V_s ratio is 1.87. The uncertainties in H and V_p/V_s are 0.47 km (~1.4%) and 0.02 (~1.1%), respectively. The maximum value of $S(H,K)$ calculated at the OZLU station indicates

that the true crustal thickness is 39.8 ± 0.34 km and V_p/V_s is 1.81 ± 0.01 . The uncertainty associated with H is ~0.85%, which is the lowest among all six stations used in this study. Likewise, the uncertainty of V_p/V_s is relatively low (~0.59%) at the OZLU station. Even though the number of the receiver functions used in analysis is the largest at station SALI, the uncertainties in both H and V_p/V_s are the highest. The best estimates of H and V_p/V_s are 38.2 km and 1.84, and the uncertainties are 1.16 km (~3.04%) and 0.03 (~1.35%), respectively.

Multiple maxima in the H-K stack suggest a laterally complex structure and a probable transition zone instead of an ordinary reflector between the crust and the mantle

Table 2. Location (coordinates and elevation), calculated arrival time of the converted Ps wave (t_{ps}), crustal thickness, crustal Vp/Vs ratio, Poisson's ratio (ν), mean crustal S-wave velocity, and the number of receiver functions used at each AnkNET station.

Station code	Lat. (°)	Long. (°)	Elevation (m)	Crustal thickness (km)	Vp/Vs	ν	Mean V_s (km/s)	No. of RFs
KSLM	39.431	33.600	1061	37.4 ± 0.6	1.80 ± 0.02	0.276	3.398	28
MRKZ	39.949	32.970	1181	34.5 ± 0.5	1.87 ± 0.02	0.300	3.575	26
OZLU	40.521	33.062	1420	39.8 ± 0.3	1.81 ± 0.01	0.279	4.117	23
SALI	40.150	32.185	956	38.2 ± 1.2	1.84 ± 0.02	0.290	3.721	34
SERE	39.302	32.596	1163	37.5 ± 0.6	1.66 ± 0.01	0.215	3.334	29
YENI	40.183	33.868	1191	40.5 ± 0.4	1.78 ± 0.01	0.249	3.958	26

beneath stations KSLM, SERE, and YENI (Figure 8). In such cases, especially if the stack amplitudes of several maxima are reasonably close, further investigations need to be made to determine the complex structure beneath the stations. Existence of a priori knowledge of the subsurface structure would help to determine the true values of thickness and Vp/Vs ratio out of multiple maxima. The global maximum of the H-K stack for KSLM is at 37.4 km in thickness and 1.80 Vp/Vs ratio with 0.6 km (~1.6%) and 0.02 (~1.11%) uncertainties while the local maximum is at 31.8 km in thickness and 2.0 Vp/Vs ratio. While the study results of Marone et al. (2003) showed that the crustal thickness near the KSLM station is almost 32 km, most previous studies (e.g., Arslan et al., 2010; Molinari and Morelli, 2011; Laske et al., 2013; Tezel et al., 2013; Vanacore et al., 2013; Uluocak et al., 2016) agreed with the crustal thickness at the global maximum. The H-K stack for SERE shows a significantly shallower Moho depth (31.4 km) and higher Vp/Vs ratio (1.87) at the local maximum than the findings of previous studies (e.g., Marone et al., 2003; Arslan et al., 2010; Molinari and Morelli, 2011; Laske et al., 2013; Tezel et al., 2013; Vanacore et al., 2013; Uluocak et al., 2016). The global maximum indicates that the crustal thickness is 37.5 ± 0.6 km and the Vp/Vs ratio is 1.66 ± 0.01 with ~1.6% and ~0.6% uncertainties, respectively. Interpretation of the H-K stack is more complicated at the YENI station. The global maximum is at 40.5 km and the local maximum is at 33.5 km of crustal thickness. The study of Vanacore et al. (2013) showed that the crustal thickness near the YENI station is nearly 37 km. Arslan et al. (2010) found crustal thickness of ~36 km near the location of the YENI station, which is almost the same in the studies of Marone et al. (2003), Tezel et al. (2013), and Uluocak et al. (2016). The crustal thickness of the same area is nearly 38.6 km in the ERcrust model of Molinari and Morelli (2011) and nearly 35.2 km in the Crust1.0 model of Laske et al. (2013). The Vp/Vs ratio at the local maximum (2.09) is far above the

ratio at the global maximum (1.78). Vp/Vs ratio findings near the location of the YENI station are between 1.8 and 1.9 in the study of Vanacore et al. (2013) and between 1.7 and 1.8 in the study of Salah et al. (2014). These results agree with the Vp/Vs ratio at the global maximum. The uncertainties at the global maximum are 0.4 km (~0.99%) and 0.01 (~0.56%) for crustal thickness and Vp/Vs ratio, respectively.

7. Discussion and conclusions

Teleseismic earthquake data recorded by the six broadband stations of a local temporary seismic network, AnkNET, were analyzed to estimate the S-wave velocity structure, crustal thickness, and Vp/Vs ratio beneath the stations. In order to obtain the crustal structure parameters mentioned before, receiver function analysis was performed for all six stations individually.

One-dimensional crustal S-wave velocity structure, the crustal thickness, and the crustal Vp/Vs ratio beneath each station were determined. The crustal S-wave velocities beneath the city of Ankara and its vicinity were found to vary between 3.3 km/s and 4.1 km/s down to 50 km in depth (Figure 6). In a previous study on the one-dimensional crustal structure of the region, Çivgin and Kaypak (2012) found that the mean S-wave velocity in the upper 30 km of depth is 3.4 km/s. The results also collaborate the estimations of Luccio and Pasyanos (2007). They found that the S-wave velocities vary between 3.5 km/s and 3.9 km/s in the crust and reach 4.4 km/s in the upper mantle beneath Central Anatolia. Saunders et al. (1998) found that the S-wave velocities beneath the ANTO station vary between 2.3 km/s and 4.5 km/s from the surface down to 40 km in depth. Erduran et al. (2007) indicated that the S-wave velocity in the near surface is 2.2 km/s and 4.27 km/s in the upper mantle beneath Anatolia. From the low S-velocity models in Figure 6, the presence of three layers can be seen. These are the sedimentary layer, the upper

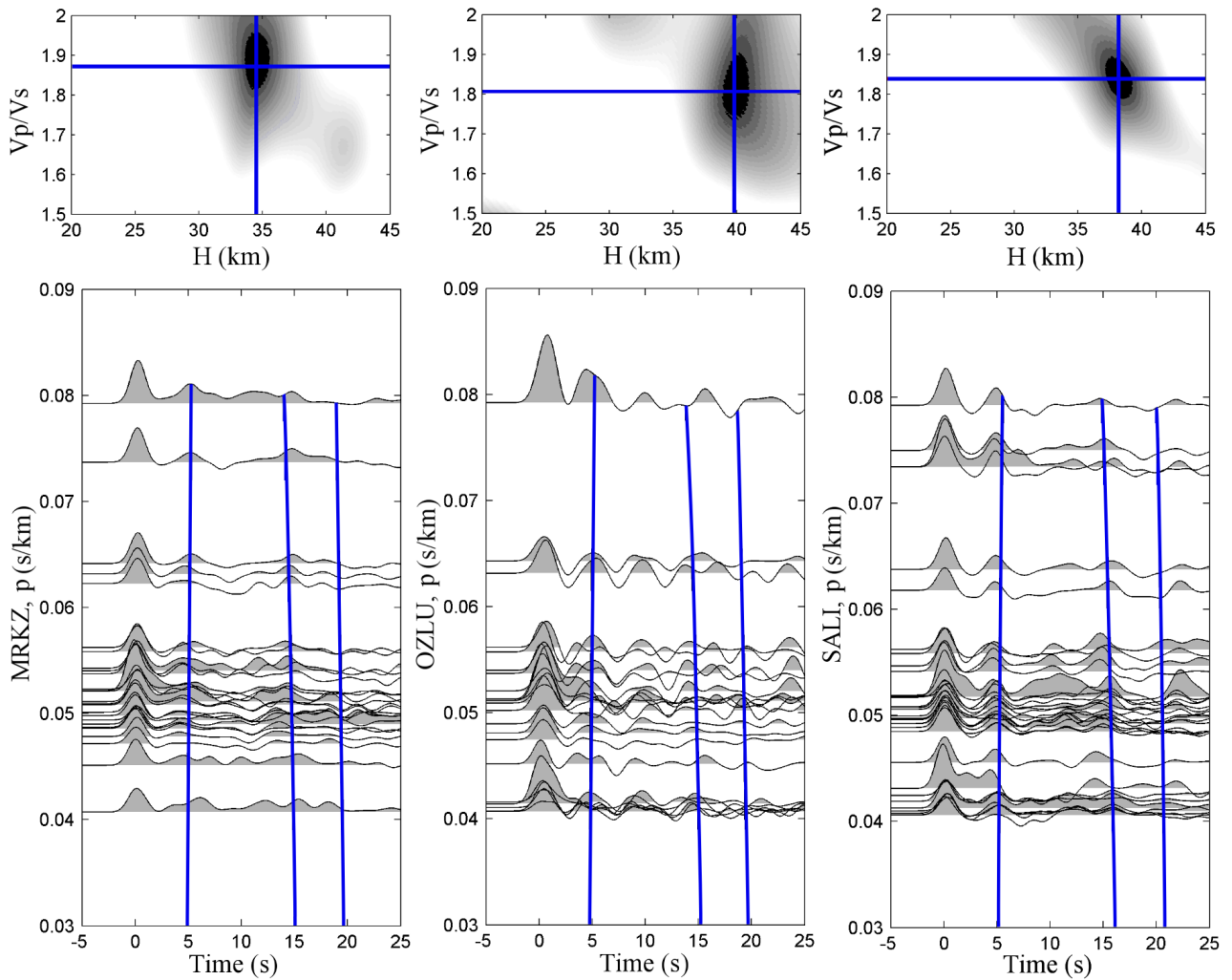


Figure 7. H-K stacks (top) for the stations MRKZ, OZLU, and SALI. The real values of H and V_p/V_s indicated clearly with a single maximum on $S(H,K)$ maps are shown with blue lines. Predicted arrival times of the converted phases are marked on the receiver function traces sorted by the ray parameter (bottom).

crust, and the lower crust. The low S-wave velocities in the near surface and their increase nearly down to 5 km in depth is clearly seen beneath every station (Figure 6), which is in good agreement with the results of Erduran et al. (2007) and Salah et al. (2014). This uppermost layer with a low S-wave velocity can be interpreted as Neogene sediments covering the whole surface of the region. The lowest sedimentary S-wave velocity (<3.0 km/s) is observed only around the SERE station. Furthermore, the stations of SALI and OZLU have thinner (below 3 km) sedimentary layers than the other stations. A typical high-velocity structure in the depth range of ~ 5 km and ~ 20 km is remarkable beneath each station, which can be associated with the upper crust. Almost all local earthquakes that occurred in the region were observed in the upper crust (Çivgin and Kaypak, 2012). Thus, we can infer that this

layer is brittle and more rigid than the lower crust. The existence of such a brittle layer can be supported by the Central Anatolia definition of Whitney and Dilek (1997) as a rigid block mainly undergoing strike-slip faulting and associated sedimentary basin development. On the other hand, Pasquarè et al. (1988) stated that the formation of Central Anatolia was dominated by great and complicated tectonic depressions. This kind of high-velocity zone was reported by various researchers (e.g., Owens, 1987; Fnais, 2004; Geissler, 2005), which are related to the intrusion or existence of high-velocity rocks in the crust. This depth range has higher S-wave velocity values (>4.5 km/s) beneath the OZLU and YENI stations, which are located on basaltic rocks. On the other hand, the S-wave velocities decrease dramatically between the depth range from ~ 20 km to Moho (Figure 6). The velocity decrement in the

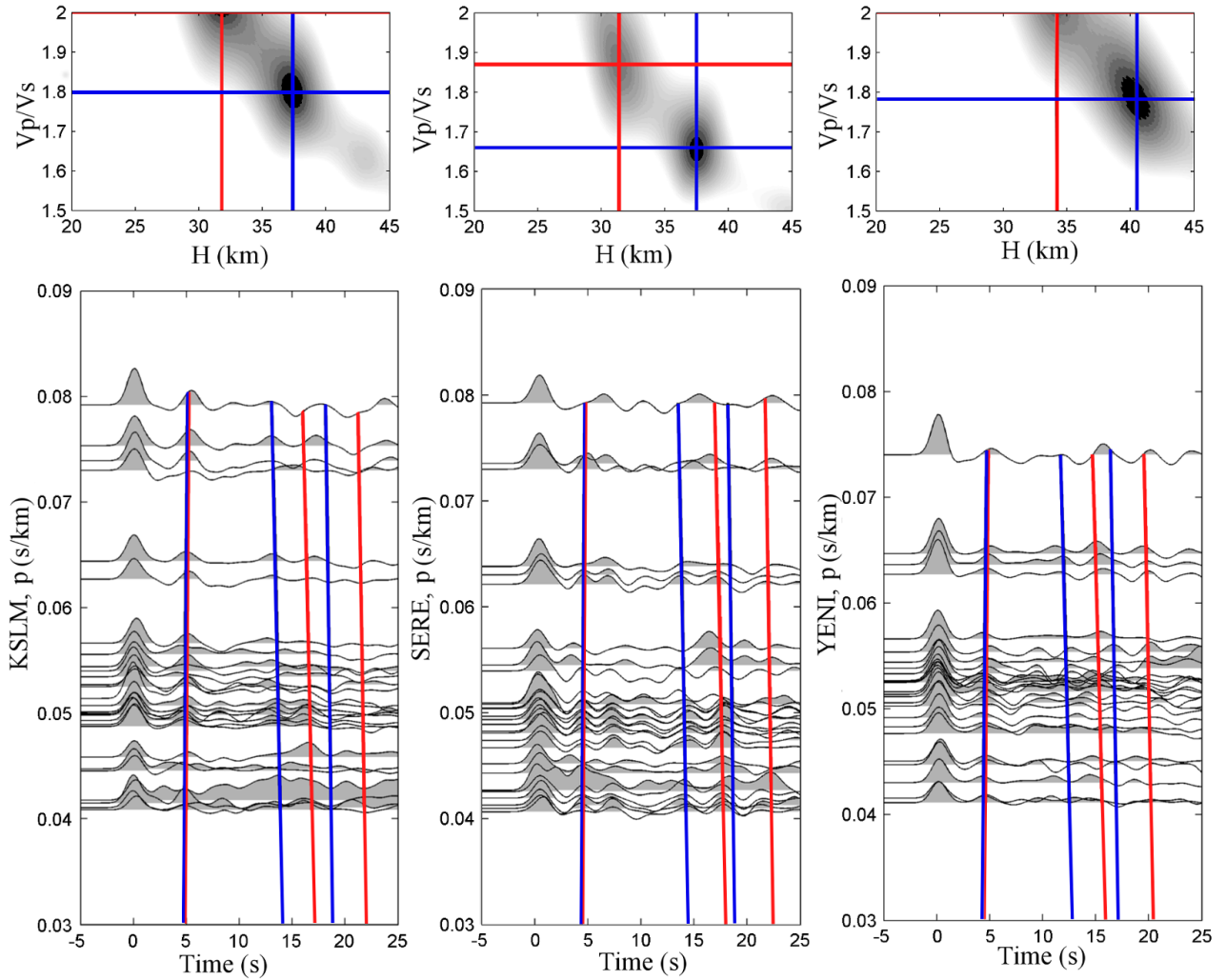


Figure 8. H-K stacks (top) for the stations KSLM, SERE, and YENI. Multiple maxima indicating the possible real values of H and V_p/V_s on $S(H,K)$ maps are shown with red and blue lines (see the text for discussion). Predicted arrival times of the converted phases for both H and V_p/V_s values from multiple maxima are marked on the receiver function traces (with corresponding colors) sorted by the ray parameter (bottom).

lower crust is observed prominently and sharply beneath some stations (KSLM, SALI, OZLU, and YENI). Most probably, the reason for the reduction in S-wave velocities in these depths is the ductile and weak structure of the lower crust because of deep heat transform. The Curie point depths at the station locations vary between 17 km and 21 km as shown in the map published by the General Directorate of Mineral Research and Exploration (MTA, 2007). According to Akın and Çiftçi (2011), the Curie point depth beneath the KSLM station is around 12.5 km, while in our model the S-wave velocity starts decreasing at almost 20 km and reaches a minimum at 23 km in depth. Bilim (2011) presented the Curie point depth map of West Anatolia, embracing the locations of the OZLU, YENI, and SALI stations. The Curie point depths are ~15 km, ~10.5

km, and ~6.5 km beneath these stations, respectively. The S-wave velocity models (Figure 6) are in good agreement with these depths. S-wave velocities start decreasing at almost the same depths of the Curie point proposed by Bilim (2011).

The estimated crustal V_p/V_s ratios vary between 1.66 and 1.87 with a maximum error of ± 0.02 . These results are mostly in good agreement with the mean crustal V_p/V_s ratios put forth by Salah et al. (2014). The crustal V_p/V_s ratio beneath the ANTO station published by Zhu et al. (2006) corroborates our findings with a value of 1.8. The results of Vanacore et al. (2013) show that the V_p/V_s ratio changes between 1.8 and 1.9 around the region. The lowest mean crustal V_p/V_s ratio is 1.66 at the SERE station, which also gives the lowest near-surface S-wave velocity.

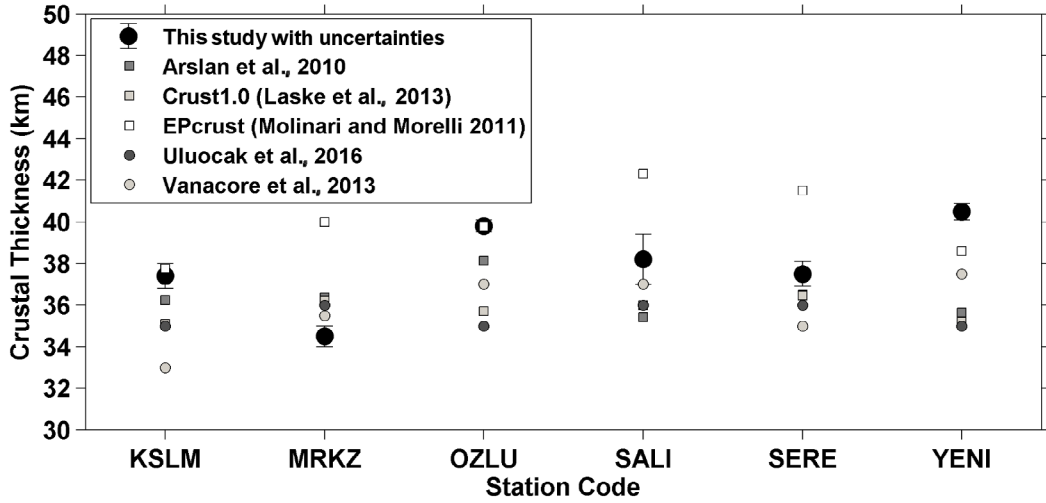


Figure 9. Comparison of the crustal thicknesses determined in this study and other studies by Arslan et al. (2010), Uluocak et al. (2016), and Vanacore et al. (2013) and the global crustal models Crust 1.0 (Laske et al., 2013) and EPcrust (Molinari and Morelli, 2011).

The estimated crustal thicknesses of the region also corroborate findings from various previous studies such as those of Türkelli (1984), Sandvol et al. (1998), Saunders et al. (1998), Gürbüz et al. (2003), Zhu et al. (2006), Luccio and Pasyanos (2007), and Tezel et al. (2013). Most studies that determined the crustal thickness beneath the ANTO station agreed on a value of almost 36 km. ANTO is located between the SERE and MRKZ stations, which gives a mean thickness of 36 km. The northernmost station OZLU and the northeastern station YENI give the largest crustal thickness values. The crust thickness map of the General Directorate of Mineral Research and Exploration of Turkey (MTA, 2017) verifies this thickening towards the north-northeast. Comparison of the crustal thicknesses determined in this study and those from some previous studies that gave the crustal thicknesses at the station locations is given in Figure 9 and discussed in Section 6 in details. Results of this study are expected to fill the

deficiency of crustal structure knowledge at the locations of AnkNET stations.

Acknowledgments

This research was funded by the Scientific and Technological Research Council of Turkey (TÜBİTAK Grant No: 2211). Data of the local temporary network were retrieved from the project “The geological and seismological investigation on the internal deformation of Anatolian Plate around Ankara”, carried out by the Tectonics Research Group of Ankara University and funded by Ankara University (Grant No: 20060745052). Computation of the receiver functions and inversion processes were performed by using Computer Programs in Seismology 3.3 software, which was developed by Herrmann (1987) and improved by Herrmann and Ammon (2002) for crustal studies. The authors appreciate the efforts made by the editor and the valuable comments of the reviewers, which made a considerable contribution to the paper.

References

- Akın U, Çiftçi Y (2011). Heat flow of the Kırşehir Massif and geological sources of the radiogenic heat production. *Mineral Res Expl Bull* 143: 53-73.
- Ammon CJ (1991). The isolation of receiver effects from teleseismic P waveforms. *Bull Seism Soc Am* 81: 2504-2510.
- Angus DA, Wilson D, Sandvol E, Ni JF (2005). Crustal and upper-mantle structure of Eastern Turkey from S-wave receiver functions. In: American Geophysical Union, Fall Meeting 2005, Abstract # S51E-1050.
- Arslan S, Akın U, Alaca A (2010). Investigation of crustal structure of Turkey by means of gravity data. *Mineral Res Expl Bull* 140: 55-71.
- Bilim F (2011). Investigation of the Galatian volcanic complex in the northern central Turkey using potential field data. *Phys Earth Planet In* 185: 36-43.
- Çıvğın B, Kaypak B (2012). Investigation of one-dimensional crustal seismic velocity structure of Ankara and surroundings. *Yerbilimleri* 33: 131-150 (in Turkish with an abstract in English).

- Erduran M, Çakır Ö, Tezel T, Şahin Ş, Alptekin Ö (2007). Anatolian surface wave evaluated at GEOFON Station ISP Isparta, Turkey. *Tectonophysics* 434: 39-54.
- Ergün M, Oral EZ, Çifçi G (1995). Eastern Mediterranean structure and its place in plate tectonics. *Jeofizik* 9-10:71-78 (article in Turkish with an abstract in English).
- Fnais MS (2004). The crustal and upper mantle shear velocity structure of eastern North America from the joint inversion of receiver function and surface-wave dispersion. PhD, Saint Louis University, St. Louis, USA.
- Geissler WH (2005). Seismic and petrological investigations of the lithosphere in the swarm-earthquake and CO₂ degassing region Vogtland/NW-Bohemia. PhD, Helmholtz-Centre Potsdam – GFZ German Research Centre for Geosciences, Potsdam, Germany.
- Goldstein P, Dodge D, Firpo M, Minner L (2003). SAC2000: Signal processing and analysis tools for seismologists and engineers. In: Lee WHK, Kanamori H, Jennings PC, Kisslinger C, editors. *The IASPEI International Handbook of Earthquake and Engineering Seismology*. London, UK: Academic Press.
- Goldstein P, Snoko A (2005). SAC availability for the IRIS community. Incorporated Institutions for Seismology Data Management Center Electronic Newsletter 7: 1. Available online at <http://ds.iris.edu/ds/newsletter/vol7/no1/sac-availability-for-the-iris-community/>.
- Gürbüz C, Bekler T, Toksöz MN, Kuleli S, Kalafat D, Schultz C (2003). Seismic refraction studies and crustal structure in Anatolia. In: Commission on Controlled-Source Seismology: Deep Seismic Methods, 12th International Workshop, Mountain Lake, VA, USA, pp. 74-78.
- Herrmann RB (1987). *Computer Programs in Seismology*. St Louis, MO, USA: Saint Louis University.
- Herrmann RB, Ammon CJ (2002). *Computer Programs in Seismology: Surface Waves, Receiver Functions and Crustal Structure, Version 3.30*. St Louis, MO, USA: Saint Louis University.
- Kind R, Kosarev GL, Petersen NV (1995). Receiver functions at the stations of the German Regional Seismic Network (GRSN). *Geophys J Int* 121: 191-202.
- Kind R, Vinnik LP (1988). The upper mantle discontinuities underneath the GRF array from P-to-S converted phases. *J Geophys* 62: 138-147.
- Langston CA (1977). The effect of planar dipping structure on source and receiver responses for constant ray parameter. *Bull Seism Soc Am* 67: 1029-1050.
- Langston CA (1979). Structure under Mount Rainier, Washington, inferred from teleseismic body waves. *J Geophys Res* 84: 4749-4762.
- Laske G, Masters G, Ma Z, Pasyanos M (2013). Update on CRUST1.0 - A 1-degree global model of Earth's crust. EGU General Assembly EGU2013-2658. Munich, Germany: EGU.
- Luccio F Di, Pasyanos ME (2007). Crustal and upper mantle structure in the Eastern Mediterranean from the analysis of surface wave dispersion curves. *Geophys J Int* 169: 1139-1152.
- Maden N, Gelişli K, Eyüboğlu Y, Bektaş O (2009). Two-and-three-dimensional crustal thickness of the Eastern Pontides (NE Turkey). *Turkish J Earth Sci* 18: 225-238.
- Marone F, van der Meijde M, van der Lee S, Giardini D (2003). Joint inversion of local, regional and teleseismic data for the crustal thickness in the Eurasia-Africa plate boundary. *Geophys J Int* 154: 499-514.
- McClusky S, Balassanian S, Barka A, Demir C, Ergintav S, Georgiev I, Gurkan O, Hamburger M, Hurst K, Kahle H et al. (2000). Global Positioning System constraints on plate kinematics and dynamics in the eastern Mediterranean and Caucasus. *J Geophys Res* 105: 5695-5719.
- McKenzie D (1972). Active tectonics of the Mediterranean region. *Geophys J R Astron Soc* 30: 190-185.
- Molinari I, Morelli A (2011). EPcrust: A reference crustal model for the European plate. *Geophys J Int* 185: 352-364.
- MTA (2007) Curie-Point Map of Turkey. Ankara, Turkey: General Directorate of Mineral Research and Exploration of Turkey.
- MTA (2017). Crust Thickness Map of Turkey. Ankara, Turkey: General Directorate of Mineral Research and Exploration of Turkey. Available online at <http://www.mta.gov.tr/eng/maps/list>.
- Owens TJ (1987). Crustal structure of the Adirondacks determined from broadband teleseismic waveform modeling. *J Geophys Res* 92: 6391-6401.
- Owens TJ, Zandt G, Taylor SR (1984). Seismic evidence for an ancient rift beneath the Cumberland Plateau, Tennessee: a detailed analysis of broadband teleseismic P waveforms. *J Geophys Res* 89: 7783-7795.
- Pasquarè G, Poli S, Vezzoli L, Zanchi A (1988). Continental arc volcanism and tectonic setting in Central Anatolia, Turkey. *Tectonophysics* 146: 217-230.
- Phinney RA (1964). Structure of the Earth's crust from spectral behaviour of long-period body waves. *J Geophys Res* 69: 2997-3017.
- Salah MK, Şahin Ş, Topatan U (2014). Crustal velocity and Vp/Vs structures beneath central Anatolia from local seismic tomography. *Arab J Geosci* 7: 4101-4118.
- Sandvol E, Seber D, Calvert A, Barazangi M (1998). Grid search modeling of receiver functions: Implications for crustal structure in the Middle East and North Africa. *J Geophys Res* 103: 26899-26917.
- Saunders P, Priestley K, Taymaz T (1998). Variations in the crustal structure beneath western Turkey. *Geophys J Int* 134: 373-389.
- Seyitoğlu G, Aktuğ B, Karadenizli L, Kaypak B, Şen Ş, Kazancı N, Işık V, Esat K, Parlak O, Varol B et al. (2009a). A late Pliocene-Quaternary pinched crustal wedge in NW Central Anatolia, Turkey: a neotectonic structure accommodating the internal deformation of the Anatolian plate. *Geol Bull Turkey* 52: 121-154.
- Seyitoğlu G, Kaypak B, Işık V, Esat K, Çivgin B (2009b). Earthquake Monitoring Network of Ankara (AnkNET). In: *International Earthquake Symposium, Kocaeli 2009 Abstracts*, p. 102.

- Tezel T, Shibutani T, Kaypak B (2013). Crustal thickness of Turkey determined by receiver function. *J Asian Earth Sci* 75: 36-45.
- Türkelli N (1984). Seismic investigation of the crustal structure in central Anatolia. PhD, Middle East Technical University, Ankara, Turkey.
- Uluocak EŞ, Pysklywec R, Göğüş OH (2016). Present-day dynamic and residual topography in Central Anatolia. *Geophys J Int* 206: 1515-1525.
- Vanacore EA, Taymaz T, Saygın E (2013). Moho structure of the Anatolian Plate from receiver function analysis. *Geophys J Int* 193: 329-337.
- Vinnik LP (1977). Detection of waves converted from P to SV in the mantle. *Phys Earth Planet In* 15: 39-45.
- Whitney DL, Dilek Y (1997). Core complex development in Central Anatolia, Turkey. *Geology* 75: 1023-1026.
- Zhu H, Kanamori H (2000). Moho depth variation in southern California from teleseismic receiver functions. *J Geophys Res* 105: 2969-2980.
- Zhu L, Mitchell BJ, Akyol N, Çemen I, Kekovalı K (2006). Crustal thickness variations in the Aegean region and implications for the extension of continental crust. *J Geophys Res* 111: B01301.